
Mining Domain Knowledge: Improved Framework towards Automatically Standardizing Anatomical Structure Nomenclature in Radiotherapy

Qiming Yang^{1,2}, Hongyang Chao^{1,2}, Dan Nguyen¹, and Steve Jiang¹

¹Medical Artificial Intelligence and Automation Laboratory, Department of Radiation Oncology, University of Texas Southwestern Medical Center, Dallas, TX, USA

²School of Data and Computer Science, Sun Yat-sen University, Guangzhou, GD, China

Corresponding author: Steve Jiang (e-mail: Steve.Jiang@UTSouthwestern.edu).

ABSTRACT Automatically standardizing nomenclature for anatomical structures in radiotherapy (RT) clinical data is an unmet urgent need in the era of big data and artificial intelligence. Existing methods either can hardly handle cross-institutional datasets or suffer from heavy imbalance and poor-quality delineation in clinical RT datasets. To solve these problems, we propose an automated structure nomenclature standardization framework, 3DNNV, which consists of an improved data processing strategy (ASAC/Voting) and an optimized feature extraction module to simulate clinicians' domain knowledge and recognition mechanisms to identify heavily imbalanced small-volume organs at risk (OARs) better than other methods. We used partial data from an open-source head-and-neck cancer dataset (HN_PETCT) to train the model, then tested the model on three cross-institutional datasets to demonstrate its generalizability. 3DNNV outperformed the baseline model (ResNet50), achieving a significantly higher average true positive rate (TPR) on the three test datasets (+8.27%, +2.39%, +5.53%). More importantly, the 3DNNV outperformed the baseline, 28.63% to 91.17%, on the F1 score of a small-volume OAR with only 9 training samples, when tested on the HN_UTSW dataset. The developed framework can be used to help standardizing structure nomenclature to facilitate data-driven clinical research in cancer radiotherapy.

INDEX TERMS Nomenclature Standardization, Radiotherapy, Deep Learning, 3D Classification, Voting

I. INTRODUCTION

In the field of radiotherapy (RT), nomenclature standardization is the process of imposing a unified, structured labeling system for anatomical structures [7, 24, 25], which is a prerequisite for clinical data curation and data-driven research especially in the era of big data and artificial intelligence [7, 26, 27, 29, 30]. Inevitably, the structure labels in clinical data are inconsistent due to differences in clinician preferences, institutional policies, vendors, and language environments [28]. For example, in the open-source head-and-neck cancer dataset HN_PETCT [12, 13], very different labels, such as "nod," "nerf optique d1," "nerf opt drt," "optcnerv(r)," "n_opt_d," and "roptic," refer to the same structure: the right optical nerve. A large number of retrospective RT datasets [23, 32] cannot be

shared and reused without consistent labels, and manual cleaning RT data requires domain knowledge and is very expensive [10, 16, 28, 38, 39]. Therefore, it's necessary to develop software tools to automate nomenclature standardization for data-driven clinical research.

Previous works have proposed standardizing the nomenclature of anatomical structures with text-based methods that rely on label matching and clinicians' intervention to correct mismatched labels to standardize RT datasets collected from a single institution in a short time [6, 10, 31]. However, language is ever-changing, and different naming conventions make the semantic information in the labels difficult to recognize automatically. As a result, text-based methods cannot be applied to datasets collected even

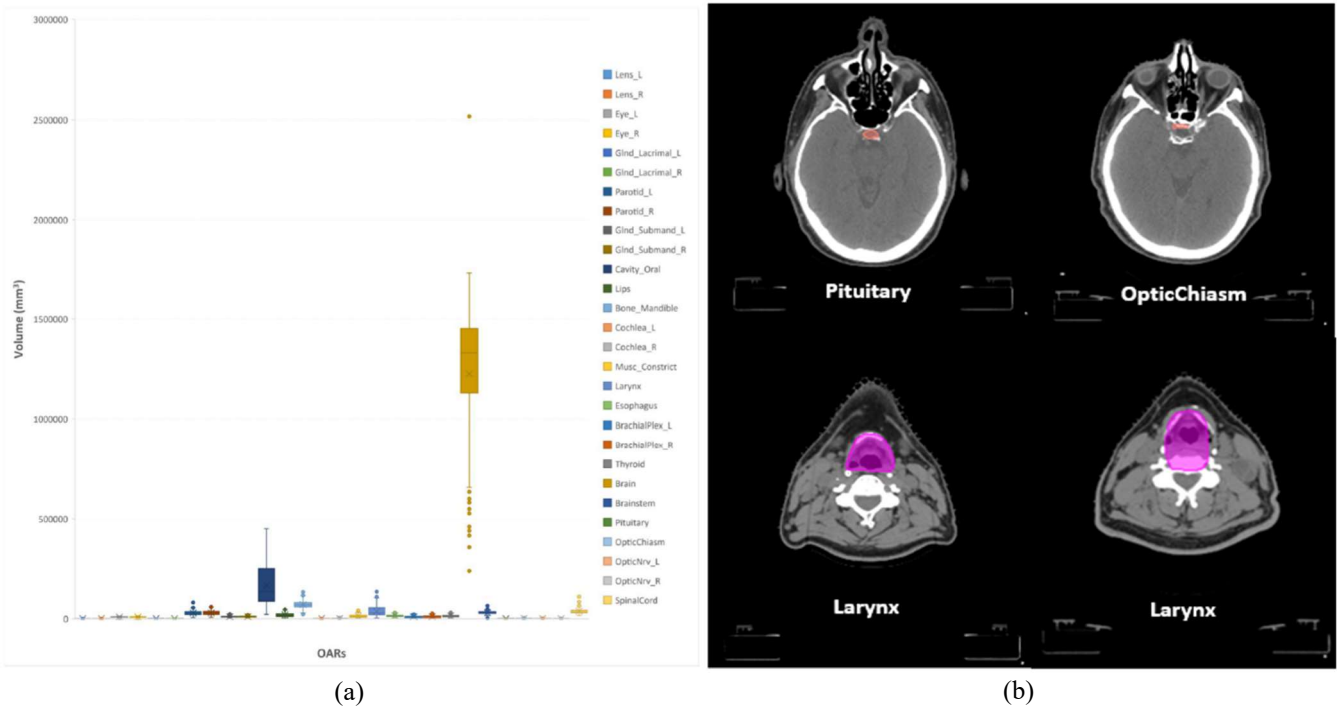


FIGURE 1. Characteristics of real RT data (HN_PETCT). (a) The size of OARs is extremely imbalanced. (b) Delineation in RT data: the first row indicates the similarity of small-volume OARs (inter-class similarity), and the second row shows examples of poor delineation for the same OAR (intra-class variation).

from a single institution, let alone to cross-institutional datasets.

The labels of organs at risk (OARs) is in one-to-one correspondence with the image (such as CT and segmentation masks), and the image data contain invariant semantic information that can standardize nomenclature in multilingual environments. Therefore, methods that leverage this image information to tackle cross-institutional RT datasets are called image-based methods. Existing image-based methods attempt to automatically standardize nomenclature by exploiting semantic invariance in the image [9, 33, 34, 35]. Among these methods, the algorithm that leverages atlas-based registration can also be used to determine the category of the structure and then to relabel it [33, 34]. However, atlas-based registration is unstable and time-consuming. Other image-based methods convert the task of structure nomenclature standardization to OAR classification based on a deep learning framework [9, 35]. Nonetheless, these methods have largely overlooked the problems caused by imbalance and poor delineation in real RT datasets, especially for small-volume OARs with similar positions, shapes, and sizes (such as pituitary and optical chiasm). Imbalance in RT datasets is not only the skew in the number of samples but also the bias in the size of the OAR. For example, in Fig. 1 (a), the volume of brain is quite different from that of pituitary. Models built on such a dataset will tend to be biased and inaccurate. Delineation for OARs become more difficult when the similarity between

categories and the difference within a category increase; for example, in Fig. 1 (b), pituitary and optical chiasm look similar while larynx looks very different for different patients. Both imbalance and poor delineation make the classifier biased, leading to incorrect predictions for small-volume OARs.

As mentioned earlier, some image-based methods treat the task of structure nomenclature standardization as an OAR classification task [9, 35]. In the field of computer vision, deep learning has led to a series of breakthroughs for classification tasks [1, 17] that have improved upon traditional classification methods [43, 44]. Related works seeking to improve the performance of DL-based classifiers have mainly focused on three aspects: 1) constructing deeper, wider, more elaborate architectures [5, 11, 17, 18, 19, 20, 21] to increase the capacity for adapting data and training [40]; 2) enriching samples to get close to the actual distribution [47, 48]; and 3) adding subjective constraints to make high-level features extracted within the network cohere with the domain knowledge required for specific tasks [41, 42, 45]. Existing state-of-the-art networks [1, 5, 11, 17, 18, 19, 20, 21] for classification can be applied to the current task. ResNet [5] has a lower computational cost but better performance than other networks [22]. Hence, we have made many attempts on the ResNet50 (see Fig. 5, Table II, Fig. 7 and Table V), which yielded results similar to previous reports [9, 35]: the true positive rate (TPR) of small-volume OARs (such as Pituitary and OpticChiasm) can't meet the requirements. It is worth noting that clinicians

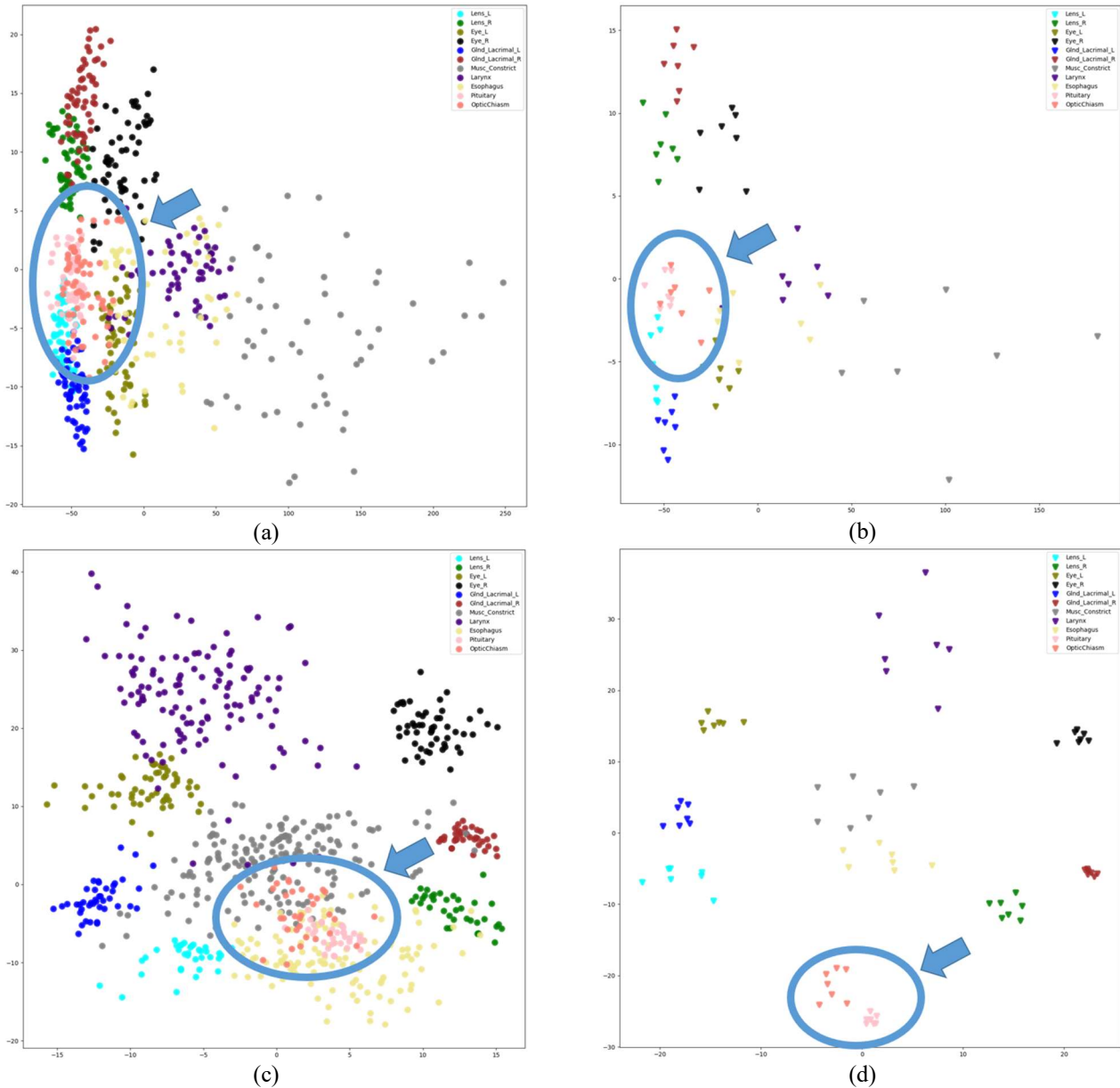


FIGURE 2. Visualization of the predictive result on the test dataset (HN_UTSW). To illustrate the performance of our work, we compared the data sampling/voting strategy proposed in TG263-Net [35] with our ASAC/Voting strategy. For each category of small-volume OAR shown in the top-right area of these figures, we randomly selected 9 samples from dataset HN_UTSW to test the models. We highlighted the results of Pituitary and OpticChiasm. (a) and (b) are the results of TG263-Net, which still confused Pituitary with OpticChiasm, while (c) and (d) show the clear boundaries between different small-volume OARs when using the ASAC/Voting strategy.

can make quick and accurate decisions for small-volume OARs, even with poorly delineated samples, which means the images contain enough effective information for clinicians to apply their domain knowledge and recognition mechanisms. How do clinicians make accurate decisions in classifying OARs? There has been no relevant research up to now. Nevertheless, we can simulate the process of clinicians observing and recognizing small-volume OARs, thus providing essential information for decision making, including implicit domain knowledge and a recognition mechanism, to the target framework. The main goal of our work is to explore

a way to integrate the domain knowledge and recognition mechanisms into a neural network from a new perspective to improve the classifier’s performance for categorizing small-volume OARs.

To this end, we propose an automatic structure nomenclature standardization framework, 3DNNV (3D Non-local Network with Voting). This framework consists of two parts: an improved data processing strategy and an optimized feature extraction structure. The data processing strategy was proposed to provide the explicit information needed by the clinician who observes the raw data and makes decisions. The

feature extraction structure simulates the observation process, which enhances the observational fineness of the region of interest (ROI) in the high-level features.

A. Improved data processing strategy

We found out that, when clinicians try to identify large-volume OARs or organs with a unique shape, they focus on the shape and location of the OARs. To categorize the error-prone small-volume OARs, clinicians need to view the whole image in a single slice (global location), then zoom in to observe the details (local details), then check the continuous slices to perceive the shape of OARs in 3D volume of CT/mask, and finally reach a decision (integrate all of these information to make a decision). The data processing strategy should provide the different information needed for large-volume and small-volume OARs. In addition, it should adaptively cope with different sizes of OARs (as shown in Fig. 1 (a)), and also take into account all information on the global location, local detail, and spatial shape when making the decision. Why not use the whole CT/mask volumes extracted from raw data and feed them into the network? Can we get a satisfactory result? With a view to the limited computation and storage resources, we can neither make unlimited augmentations to the samples, nor directly feed all of the raw data into the network. After normalizing the voxel size, the CT volume may reach $600 \times 512 \times 512$, stored as 64-bit floating type, and the size is about 1.2 GB. The computational and storage costs would be too great. We noted that clinicians could identify OARs without going through every slice, which means that several continuous slices in the vertical CT/mask direction contain enough information to distinguish OARs. Moreover, Geirhos et al. [41] have shown that, even with sufficient training data and a well-performing network, the semantic features and decision-making mechanisms learned by the trained model are likely differ from human cognition. That's why we need to integrate domain knowledge and recognition mechanisms into the network. To tackle the aforementioned challenges and provide the explicit information required by clinicians to make decisions, we propose a simple and effective adaptive data processing strategy: ASAC (adaptive sampling and adaptive cropping) and voting. ASAC adaptively simulates the process of clinicians observing images and collecting the information needed for decision making, and it generates multi-scale and multi-position inputs for a sample. ASAC constructs a set of augmented inputs with subjective constraints, assists the model in mining the effective information implicit in the raw data, and extracts the domain knowledge that clinicians needed to identify the OARs. However, inputs from the same category, even from the same sample, contain different locations and shapes and may be poorly delineated, which makes a difference in semantic feature distributions (as shown in Fig. 2 (c)). Such inputs can be regarded as approximations of the "ideal" semantic features. To compensate for the disturbance in semantic feature distribution and to assist the

model in deciding between the predictive results obtained from different inputs, we proposed a voting strategy and applied it in the inference phase. The voting strategy is a weighted sum of all the predictive results of inputs for the same sample that makes the final result closer to predicting the "ideal" semantic features (as shown in Fig. 2 (d)). The voting strategy also accords with the principle of clinicians making decisions based on comprehensive information.

B. Optimized feature extraction structure

The convolutional network only processes one local neighborhood at a time, and the common way to model the long-range dependency on semantic features is to increase the receptive field. In order to fill in the gaps in capturing long-range dependency and to enhance the observational fineness in the region of interest in the high-level semantic features, we added non-local blocks [15] to ResNet50 to optimize the feature extraction structure in the network (so-call Non-local Network, NN). Non-local blocks apply a self-attention mechanism [14] to image sequence processing by calculating the similarity matrix for high-level semantic features, thereby containing the long-range dependency and enhancing the representation of the semantic features.

By combining the ASAC/Voting strategy with the Non-local Network, we obtained the final framework, 3DNNV (3D Non-local Network with Voting), which is capable of standardizing the nomenclature of structures in RT datasets. The 3DNNV integrates clinicians' domain knowledge and recognition mechanisms into the final model from a new perspective, mitigates the problems caused by imbalance and poor delineation in RT datasets, and improves the performance for identifying small-volume OARs. This framework allows us to categorize structures in cross-institutional RT data quickly and efficiently, then automatically relabel these structures with general labels recommended in AAPM TG-263 [7]. The experimental results comparing 3DNNV against the baseline ResNet50, which serves as its backbone, show that 3DNNV significantly outperformed the baseline in identifying small-volume OARs, and the F1 score of Pituitary and OpticChiasm increased from 28.63% and 86.35% to 91.17% and 99.47%, respectively. What's more, 3DNNV is extensible and can be easily transferred to other anatomic sites after fine-tuning on a few samples.

II. RELATED WORK

A. Text-based methods

Text-based methods standardize structure nomenclature mainly using structured naming templates or label mapping dictionaries. Initially, Mayo et al. [6] built software containing structured templates, which allows clinicians to relabel the structures interactively. The fixed template helps to unify

labels better than free-text interactive tools. Nyholm et al. [31] mapped the main structure labels in the local clinical center to the name list of the general naming convention, then manually corrected the mismatched labels through the interactive interface. The authors aggregated RT data collected from 15 medical centers in Sweden using the tool. Recently, Schuler et al. [10] pointed out that, in the process of standardizing radiotherapy data, it is difficult to distinguish between typographic name variations and fundamental semantic differences in the same structure. Therefore, they developed a tool called Stature that maps a local standard structure name (LSSN) to the AAPM TG 263 naming table by creating a lookup dictionary. The above methods map the original labels to standardized labels based on a dictionary and manual intervention. These kinds of methods can establish the mapping between the original labels and standardized labels and solve the problem of inconsistent labels in the local RT dataset in a short time. However, language is ever-changing,

as shown in Table I, which limits the applicability of text-based methods to cross-institutional datasets. What's more, the text-based methods cannot handle large-scale retrospective datasets.

TABLE I
INCONSISTENT LABELS IN HN_PETCT. THERE ARE VERY DIFFERENT LABELS FOR THE SAME OARS, SUCH AS "NOD" AND "NERF OPT DRT."

Patient 1	Patient 2	Patient 3
Parotide D	RT Parotid	PAROTIDE D
GTVggIIID	Mandible	MANDIBULES
Ext 0.5	LT Eye	PLEXUS BR D
nerf opt drt	Cord	NOD
Moelle	LT	GL LACR D
	SUBMANDIBULAR	
Oeil gche	GTV	CERVEAU-
Cerveau	CTV1	NUQUE
External	EXTERNAL	CONF_1PTV3
pt pr	Midline	5412(1DMPO1.1)_1
Tronc cerebral	Brainstem	PEAU
Cristallin G	LT Parotid	CRISTAL G

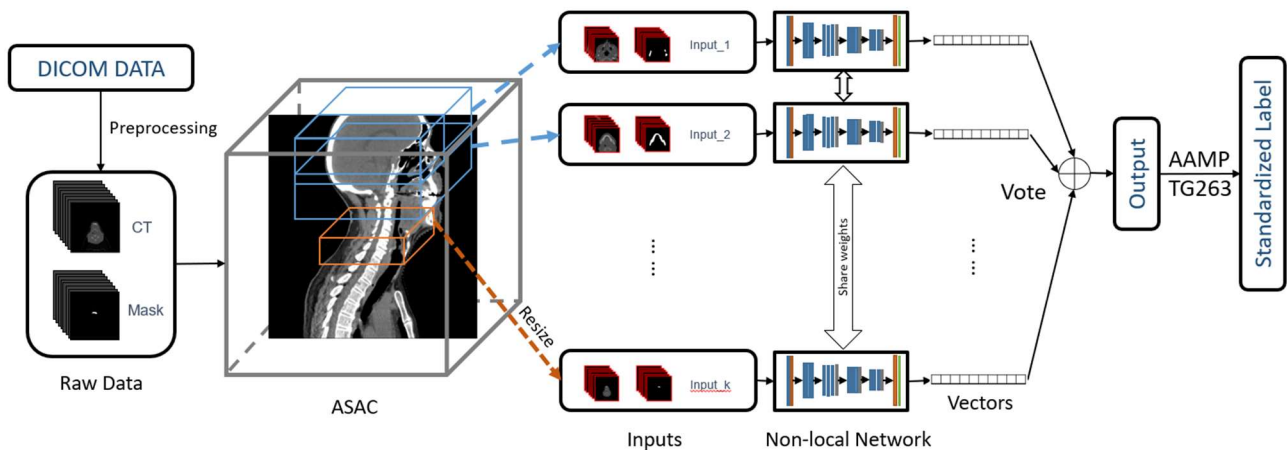


FIGURE 3. Overview of 3DNNV in the inference phase.

B. Image-based methods

Image-based methods, which are based on the invariant semantic information in medical images, are learnable automatic recognition methods that overcome the problems inherent in the text-based methods. The label propagation, which is implemented by an atlas-based deformable image registration (DIR) algorithm, registers an atlas with known labels to input and then chooses the one with the highest overlap mask to relabel the input [34]. In this way, unknown datasets can be standardized by labels in the atlas. However, the performance of the DIR is unstable [33]. Also, it's highly time-consuming, so it falls well short of practical requirements. Our previous work converted label standardization to the task of automatically categorizing structures in RT data and modeled the process with a deep

neural network, which used the weighted mask of OARs to construct a composite mask as 2D input [9]. This work demonstrated the excellent performance of deep learning networks in standardizing OAR labels, but the experiment did not make full use of the three-dimensional shape and location information on the CT. The classes of OARs in the training dataset are clean and sufficient, but the real dataset contains many other challenges, such as heavy data imbalance, inter-class similarity, and intra-class variation, etc., that may limit the method when extending to other anatomic sites. Further, Rhee et al. [35] extended the number of categories to 19 OARs in the head-and-neck region and loosely utilized the encoder of V-Net [36] to construct their framework, TG263-Net, which leveraged 3D inputs and achieved high accuracy in identifying 19 OARs. But they did not take into account the

imbalance and poor delineation in RT datasets, so their performance on identifying small-volume OARs is insufficient for practical clinical needs.

III. MATERIALS AND METHODOLOGY

A. Overview of 3DNNV

In this section, we outline the workflow of 3DNNV, as shown in Fig. 3. 3DNNV consists of two parts in the inference phase for structure nomenclature standardization: 1) ASAC/Voting strategy and 2) Non-local Network. For any OAR in given DICOM data, the CT and corresponding mask are extracted to form a raw data pair. Then, ASAC generates multi-scale and multi-position inputs for each sample. During training, each input generated by ASAC is regarded as an independent sample, and the parameters of the non-local network are updated and optimized based on the samples in each mini-batch. In the inference phase, multiple inputs for a sample are fed into the network, the outputs vote for a final predictive result as the output of 3DNNV, and the sample is renamed with a standardized label.

B. Data

According to the suggestion in Brouwer et al. [3], we selected 28 categories of OARs (as shown in Fig. 1 (a): Lens_L/R, Eye_L/R, GlnD_Lacrimal_L/R, Parotid_L/R, GlnD_Submand_L/R, Cavity_Oral, Lips, Bone_Mandible, Cochlea_L/R, Musc_Constrict, Larynx, Esophagus, BrachialPlex_L/R, Thyroid, Brain, Brainstem, Pituitary, OpticChiasm, OpticNrv_L/R and SpinalCord) in the head-and-neck region to train our model. To compare our model's performance in standardizing structure nomenclature against other models, we tested the models on three different head-and-neck image datasets.

1) HN_PETCT

HN_PETCT [12, 13] is an open-source head-and-neck RT dataset released on TCIA [4] that includes data collected from 4 different French medical institutions comprising 298 patients. For the 28 OARs, 4372 samples were collected in total. Then, the samples were divided into three subsets for training, validation, and testing in a ratio of 3:1:1. It should be noted that the number of samples in the dataset is extremely imbalanced. For GlnD_Lacrimal_L/R and Pituitary, only 9 samples were used as training data.

2) PDDCA

PDDCA [8] is an open-source RT dataset containing data from 48 patients, released by the MICCAI 2015 Segmentation Challenge. This dataset contains only 9 categories of head-and-neck OARs (Parotid_L, Parotid_R, GlnD_Submand_L, GlnD_Submand_R, Bone_Mandible, Brainstem, OpticChiasm, OpticNrv_L, and OpticNrv_R). All contours for OARs were re-delineated by trained radiologists. In total, 408 samples were collected, all of which were used as a test set.

3) HN_UTSW

HN_UTSW is an RT dataset collected by our team that contains data for 408 patients. We collected a total of 5153

samples for 28 OARs (the same as HN_PETCT), all of which were used for testing to show our model's generalizability.

C. Preprocessing

For each patient's data in given DICOM files, 3D CT volumes and corresponding masks were extracted to form raw data, then the voxel size of the 3D volumes in the raw data was normalized. To ensure that the small-volume OARs did not lose any information during the process of interpolation, we chose the smallest spacing ratio from the different voxel sizes in training dataset HN_PETCT—i.e., vertical voxel size: horizontal voxel size = 0.7680098:1—as a standard ratio. We performed trilinear interpolation for resizing and reshaping. Due to wide differences in Hounsfield unit (HU) values, the range of HU values was truncated to [-1000, 2500], then normalized to [0, 1]. We directly used a binary [0, 1] matrix to represent the mask. In general, the mask should be continuous on the vertical axis, but because some of the samples lacked an intermediate mask, we used the nearest mask to fill in the missing slice in such cases.

D. 3DNNV

ASAC/Voting was proposed in this work as an essential part of 3DNNV. It is worth noting that ASAC is a data processing strategy that can be applied in all stages, while the voting strategy is applied only in the inference phase.

1) ASAC: ADAPTIVE SAMPLING AND ADAPTIVE CROPPING

As shown in Fig. 1 (a), there are huge differences in the sizes of head-and-neck OARs. Directly feeding the entire CT and mask volumes into the neural network would be expensive, in terms of computation and storage. ASAC is not only a way to extract clinicians' domain knowledge but also a way to unify input data under conditions of limited computational resources and an imbalanced training dataset. For each pair of pre-processed 3D CT and mask volumes, the same processing steps were adopted: a sliding cube was set to slide in the vertical axis direction, and the cube of size $n \times m \times m$ was adaptively and intermittently cropped. For our experiments, we set 5 scales for the cropping cube: $12 \times 128 \times 128$, $18 \times 192 \times 192$, $24 \times 256 \times 256$, $30 \times 320 \times 320$, and $36 \times 384 \times 384$. After normalizing the voxel size of each volume in the raw data, every pixel in the volumes had the same ratio in shape, so we set the sampling interval distance between slices as $\text{interval} = n / 3 \times 2$, and slid the cube to extract the inputs vertically. We collected different scales of samples, then resized all of them to $12 \times 128 \times 128$, which yielded the final inputs for 3DNNV. The process of extracting samples is shown in Fig. 3. To avoid losing effective information, the process of extracting small-volume OARs does not include any down-sampling operations. For some oversized OARs, such as Brain, the contour on the horizontal slice cannot be completely cropped by small-volume cubes. Therefore, it is necessary to adaptively resize the CT and mask first to fit them into the cubes, and then perform the sampling. After

performing ASAC, we gained multi-scale and multi-position inputs for each sample.

2) VOTING

Voting strategies in deep learning are mostly applied in ensemble networks, which combine multiple networks to optimize the final decision [2]. But the shortcoming of ensemble networks is that it takes extra time to train multiple networks. In our proposed framework, we leverage ASAC to generate multi-scale and multi-position inputs, which contain different global location and local detail information. To make full use of these multi-scale and multi-position inputs, and to weaken the disturbance between different

inputs for a sample, we combine all the inputs of the same OAR sample to vote for the final recognition result in the inference phase. In this phase, a pair of inputs and outputs for the network is marked as (x_k, y_k) , $k \in [1, K]$, where x and y represent the input and ground-truth label of the k -th sample in the dataset, and there are K samples in the dataset in total. For any sample x_k , \hat{y}_k is the predictive result, and ASAC will generate multiple inputs for it, denoted by $x_k^{S_{ij}}$, which means the j -th input generated in scale S_i , $i \in [1, N]$, $j \in [1, M]$. ASAC generates multi-scale and multi-position inputs for

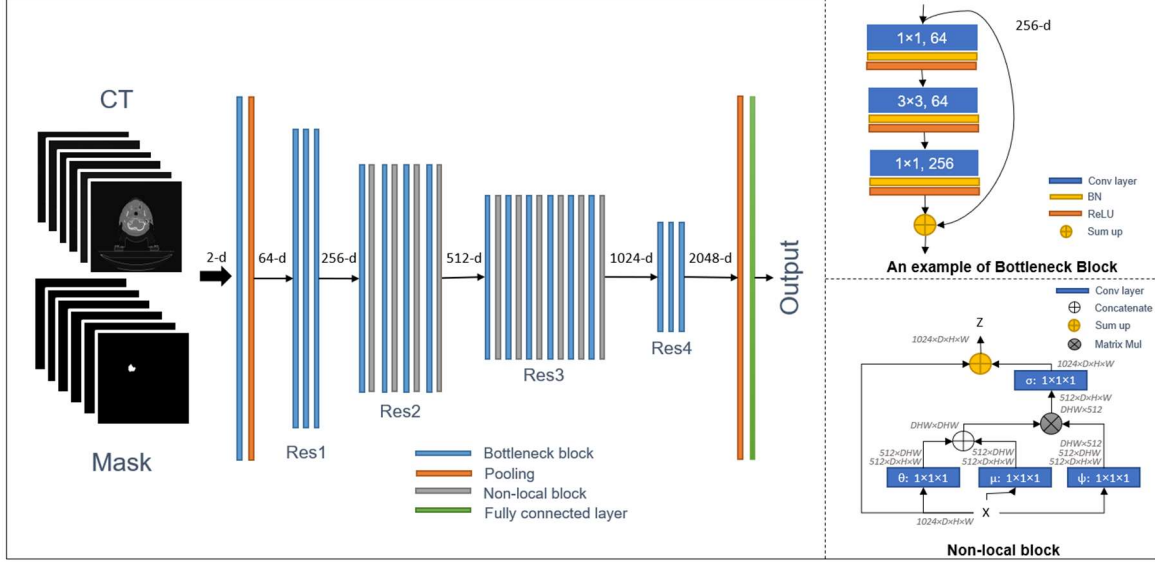


FIGURE 4. Non-local Network.

different OARs adaptively, so the number of inputs in a specific scale cannot be guaranteed; in this paper, $N=5$, $M \geq 1$. We set the cross-entropy function as the objective function, denoted as L_{CE} .

$$\hat{y}_k = \text{Network}(x_k^{S_{ij}}) \quad (1)$$

$$L_{CE}(\hat{y}_k, y_k) = -\sum y_k \log(\hat{y}_k) \quad (2)$$

In the training phase, for any batch containing input $x_k^{S_{ij}}$, the loss is calculated independently (as shown above), then the parameters of the networks are updated in backpropagation.

$$\hat{y}_k = 3DNNV(x_k) \frac{1}{T} \sum_i^N \sum_j^M \text{Network}(x_k^{S_{ij}}) \quad (3)$$

In the test phase, all inputs of a single sample x_k are combined to vote for the final prediction result. T is the total number of all inputs for x_k .

3) NON-LOCAL NETWORK

We set vanilla ResNet50 as the backbone network and also as the baseline model mentioned in Table II. Then, we added non-local blocks [15] to the backbone network to form the final 3D non-local network, as shown in Fig. 4. Inspired by the self-attention mechanism [14], the non-local block was proposed by Wang, et al. [15] to capture the global dependence in semantic features. It's designed to handle sequential data, so we stacked it into our framework. In this work, we are committed to enhancing the position information's dependence on the CT image and the shape information's dependence on the mask image, so the pairwise function f may be implemented using the concatenated form. The non-local block used in our network is defined as follows:

$$y_i = \frac{1}{C(x)} \sum_j f(x_i, x_j) \psi(x_j) \quad (4)$$

$$f(x_i, x_j) = \text{ReLU}(W_f^T[\theta(x_i), \mu(x_j)]) \quad (5)$$

$$z_i = \sigma(y_i) + x_i \quad (6)$$

x and z are set as the input and output, respectively, of the non-local block. Both are in the same size of $B \times C \times D \times H \times W$. B denotes the batch size of the input, and C represents the number of channels. D , H , and W are depth, height, and width, respectively. Here, i is the index of an output position whose response is to be computed, j is the index of all possible positions, and y is an intermediate output with the same size as x . All of ψ , θ , μ , and σ are $1 \times 1 \times 1$ convolution layers. Operator $[.,.]$ indicates the concatenation operation, and W_f is the mapping matrix that converts the concatenated vector to the scalar output. “ $+x_i$ ” indicates identity mapping, and the input x_i is added to the transformed y to get the final output z of the non-local block. $C(x)$ is a regularization term: $C(x) = D \times H \times W$.

IV. EXPERIMENTS

A. Experimental setting

1) IMPLEMENTATION DETAILS

During the training phase, we oversampled the underrepresented OARs to reduce the impact of the imbalanced training data. We performed affine transformations to augment the training data, including randomly translating, rotating, shearing, and scaling, then we cropped the central cube of the sample as input data; all of these transformations were implemented on the fly. The final input data size was $2 \times 12 \times 96 \times 96$, which is two-channel 3D data that includes the 3D CT volume and the corresponding mask on the same slices. 3DNNV was implemented on the PyTorch 1.0 framework and trained on a single GPU NVIDIA Tesla K80. All architectures used in this work were initialized as described by He et al. [37]. We adopted Adam [46] to optimize the networks with an initial learning rate of $1e-4$. Batch size was set to 16. For samples generated by ASAC, we set the total number of epochs to 20, and the learning rate dropped by a factor of 10 after 2, 5, and 10 epochs. For other architectures without ASAC, we set the total number of epochs to 200, and the learning rate decreased by a factor of 10 after 10, 20, and 30 epochs. Here, we used cross-entropy loss as the optimization objective function (as shown in (5)).

2) EVALUATION

In this multi-class classification task, we used TPR (true positive rate), F1 score, and AUC (area under the receiver operating characteristic curve) to evaluate the performance of our models, defined as follows:

$$\text{TPR} = \frac{TP}{TP+FN} \quad (7)$$

$$\text{PPV} = \frac{TP}{TP+FP} \quad (8)$$

$$\text{F1} = 2 \cdot \frac{\text{PPV} \cdot \text{TPR}}{\text{PPV} + \text{TPR}} \quad (9)$$

$$\text{AUC} = \frac{\sum_{\text{ins}_i \in \text{positive}} \text{rank}_{\text{ins}_i} - \frac{M \times (M + 1)}{2}}{M \times N} \quad (10)$$

Multi-class classification can be considered as multiple binary classifications and can calculate TP (true positive), FN (false negative) and FP (false positive) for each category separately. F1 score is the harmonic mean of PPV (positive predictive value) and TPR. In (10), $\text{rank}_{\text{ins}_i}$ means the i -th positive sample sorted by probability. AUC indicates how well the model can distinguish different classes. AUC is not sensitive when used on the imbalanced test sample.

B. Comparisons with ResNet

Under conditions where sufficient clinical data cannot be obtained, optimizing the architecture of the network and making full use of domain knowledge are the keys to improving the performance of the classification algorithm. Hence, we set vanilla 3D ResNet50 as the backbone network and tried to optimize the architecture and learn domain knowledge from raw data. To compare the performance of different data processing strategies in the experimental results, we set global samples (GS), local samples (LS) and the samples generated by ASAC for different architectures. The samples collected at the scale of $12 \times 128 \times 128$ were marked as local samples (LS), and the samples collected at the scale of $36 \times 384 \times 384$ were global samples (GS). VN means voxel normalization. Fig. 5 and Table II show that, for the error-prone small-volume OARs in the head-and-neck region, detailed information contained in the local sample plays an important role in recognition. Local details are beneficial for a model to classify small-volume OARs. However, for some patients' data, the model trained on the local sample was unable to identify BrachialPlex_L (BP_L) or BrachialPlex_R (BP_R); Fig. 6 shows the same thing happening for Baseline (VN-LS) and NN (VN-LS). Without the global location information, the model failed to indicate on which side the OAR should be.

In order to enhance the representation of small-volume OARs in high-level feature space, we added non-local blocks to the backbone network and compared the results of the non-local network (NN) with the baselines. The NN performed slightly better than the baselines, especially for Pituitary and OpticChiasm. The proposed framework, 3DNNV, which is a non-local network that is trained on the samples generated by ASAC and that votes for a final predictive result in the inference phase, performed well in identifying small-volume OARs, even those similar in shape, size and location, such as Pituitary and OpticChiasm.

Likewise, we obtained the evaluation results of 28 OARs on the three cross-institutional test sets. As shown in Table III, 3DNNV is superior to the baseline methods for classifying OARs and has good generalizability across different institutional datasets.

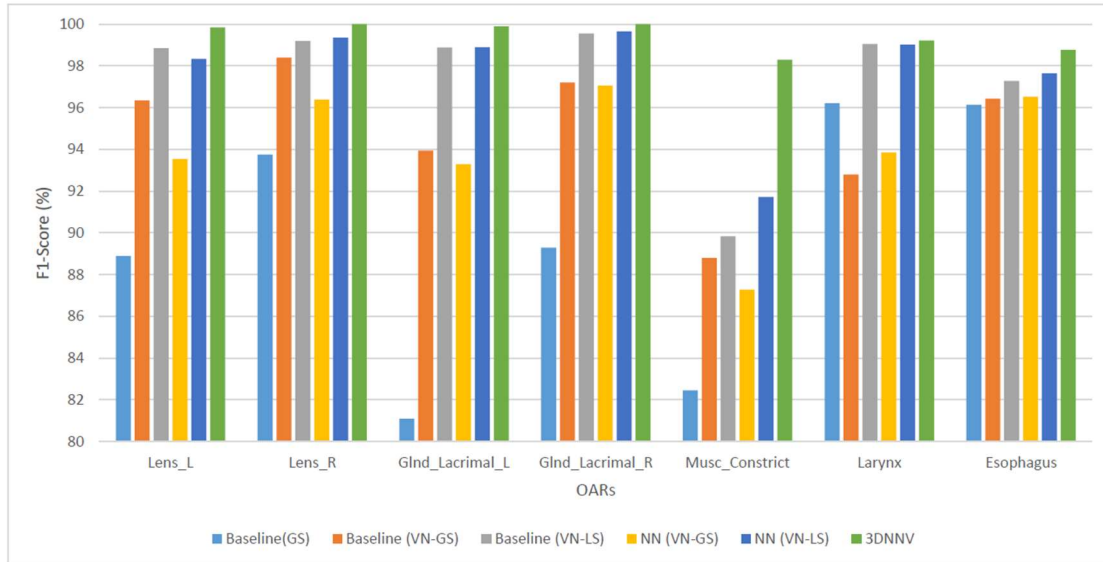


FIGURE 5. Average F1 Score (%) for small-volume OARs in HN_UTSW.

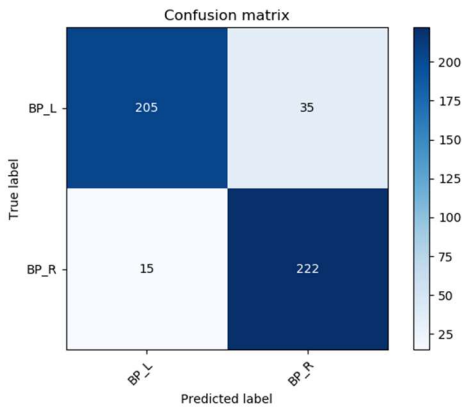


FIGURE 6. Confusion matrix of Baseline (VN-LS) on BrachialPlex_L and BrachialPlex_R.

TABLE II
AVERAGE F1 SCORE (%) OF PITUITARY AND OPTICCHIASM ON HN_UTSW.

Architecture	Pituitary	OpticChiasm
Baseline (GS)	28.63±8.33	86.35±4.06
Baseline (VN-GS)	61.87±18.73	96.83±1.91
Baseline (VN-LS)	42.61±10.87	90.41±2.38
NN (VN-GS)	82.05±15.77	98.32±0.97
NN (VN-LS)	59.26 ± 8.83	95.41 ± 1.73
3DNNV	91.17±3.18	99.47±0.18

TABLE III
EVALUATION OF BASELINES, NN AND 3DNNV ON THREE DIFFERENT TEST DATASETS.

Architecture	HN PETCT			PDDCA			HN UTSW		
	TPR	F1	AUC	TPR	F1	AUC	TPR	F1	AUC
Baseline (GS)	91.54±17.13	91.61±15.96	95.72±8.59	97.61±5.02	98.51±3.22	98.79±2.55	93.36±9.61	91.81±13.28	96.60±4.82
Baseline (VN-GS)	95.33±10.71	95.83±9.00	97.64±5.36	99.04±2.08	99.43±1.10	99.51±1.03	96.54±5.29	95.75±7.13	98.23±2.65
Baseline (VN-LS)	98.56±2.49	98.72±1.93	99.26±1.25	97.79±6.40	98.69±3.73	98.89±3.20	96.03±6.04	93.96±12.18	97.96±3.07
NN (VN-GS)	96.07±7.97	96.27±7.36	98.00±3.99	98.96±3.12	99.45±1.65	99.48±1.56	96.56±5.15	96.53±4.05	98.24±2.58
NN (VN-LS)	98.71±1.71	98.64±1.54	99.34±0.85	99.05±2.22	99.51±1.16	99.53±1.11	96.65±5.20	95.57±8.31	98.27±2.64
3DNNV	99.81±0.63	99.82±0.39	99.90±0.31	100±0	100±0	100±0	98.87±2.37	98.90±1.91	99.42±1.19

C. Comparisons with previous works

This section shows the performance comparisons between 3DNNV and the other image-based methods we applied to structure nomenclature standardization.

1) ATLAS-BASED REGISTRATION

We verified the performance of an atlas-based registration algorithm on standardizing the nomenclature of structures. To reduce the cost of computation and the complexity of the

optimization process, we constructed a 2D single-atlas database for 28 OARs, each of which contains a CT slice and a mask for the OAR to be identified in the same slice. For each pair of fixed CT and fixed mask of the OAR to be identified, we registered the moving CT in each atlas to the fixed CT, fit the transformation, and then calculated the overlapping area of the transformed moving mask and the fixed mask, using DSC (Dice similarity coefficient) to evaluate. DSC is shown in the following formula, with X and Y denoting the mask images to be compared.

$$\text{DSC} = \frac{2|X \cap Y|}{|X| + |Y|} \quad (11)$$

We selected the atlas with the highest overlap to the given fixed mask, then assigned the atlas label to the OAR to be identified to get the label standardization result.

Additionally, before being fed into 3DNNV, every structure was processed by an early-match module, which aims to avoid processing standardized structures repeatedly. The early-match module performs string matching between the original label and the standardized label: if and only if the original label fully matched one of the standardized labels in the dictionary, then the original label was treated as an already standardized label. Because we were limited by running time, we randomly selected two patients' data from the HN_UTSW dataset for testing. The results are shown in Table IV:

TABLE IV
RESULTS OF TESTING ON 2-PATIENT DATA

Evaluation (Positive/All, Time)	Patient 1	Patient 2
Atlas-based registration	13/14, 19m 34.25s	7/24, 32m 35.67s
3DNNV w/ early-match	14/14, 32.94s	23/24, 1m 19.86s

The results show that the atlas-based registration algorithm is very time-consuming and unstable on different patient data sets, and its running time is almost 30 times longer than 3DNNV's, which is unacceptable for this application. The registration effect of atlas-based deformable image registration often depends on the atlas dataset, the deformation model and the objective function, but it is difficult to construct an optimal single-atlas database. Multi-

atlas datasets could be applied to make up for this deficiency, but this would be even more time-consuming.

2) DL-BASED METHODS

We adopted different deep-learning architectures of networks and inputs for this task. For the different inputs used in this section, *1c2d* means a 1-channel composite mask [9], *2c2d* is a 2-channel input combining 2D CT and corresponding mask, and *2c3d* is a 2-channel 3D CT and mask [35]. For different architectures, we trained and tested 5-layer CNN [9], vanilla 2D ResNet50 [5], and TG263-Net [35] on the same datasets and compared their performance with 3DNNV. We delved into details for the small-volume OARs, which suffered from poor delineation and an imbalanced dataset. Fig. 7 and Table V indicate the different models' performance on cross-institutional datasets. The experimental results show that the data processing strategy plays an important role in constructing a classification network: the more effective the information contained in the inputs, the better the performance. However, the information contained in the 1c2d or 2c2d inputs cannot handle 28-OAR categorization. For the OARs with similar shape and size, 5-layer CNN with a composite mask model tends to be confused (Fig. 7 and Table V).

For TG263-Net [35], we loosely used the encoder in V-Net [36] to construct the classifier. We normalized the voxel size of CT and mask volumes in raw data to 2 mm : 2 mm : 2 mm and cropped the central cube to 64 × 64 × 64 of corresponding OARs to construct the 2-channel input. We randomly translated the center-of-mass by 10 mm to gain 9 inputs for each sample. In the inference phase, the 9 samples voted for a final prediction result. This sampling strategy is similar to 3DNNV to some extent, so we applied the same sampling strategy (also the voting strategy) as our Non-local Network (NN) used in 3DNNV. Fig. 7 and Table V compare the results of TG263-Net (2c3d) and NN (2c3d), which used the same data processing and voting strategies, and the results of NN (2c3d) and 3DNNV, which trained on the same network. We know that the data processing strategy can matter a lot, especially for identifying small-volume OARs. We found that the TG263-Net and Non-local Network models without ASAC could

TABLE V
AVERAGE F1 SCORE (%) OF PITUITARY AND OPTICCHIASM ON HN_UTSW

Architecture	Params (M)	FLOPs (G)	Pituitary	OpticChiasm
5-layer CNN [9] (1c2d)	34.71	1.74	0.00 ± 0.00	30.61 ± 5.49
ResNet50 [5] (1c2d)	24.03	1.32	0.00 ± 0.00	39.55 ± 5.30
5-layer CNN [9] (2c2d)	34.71	1.74	0.00 ± 0.00	3.49 ± 4.81
ResNet50 [5] (2c2d)	24.03	1.32	7.99 ± 5.84	58.44 ± 16.88
TG263-Net [35] (2c3d)	48.91	25.36	52.07 ± 18.41	92.92 ± 2.75
NN (2c3d)	69.83	7.85	20.78 ± 10.03	75.96 ± 12.59
3DNNV	69.83	7.24	91.17±3.18	99.47±0.18

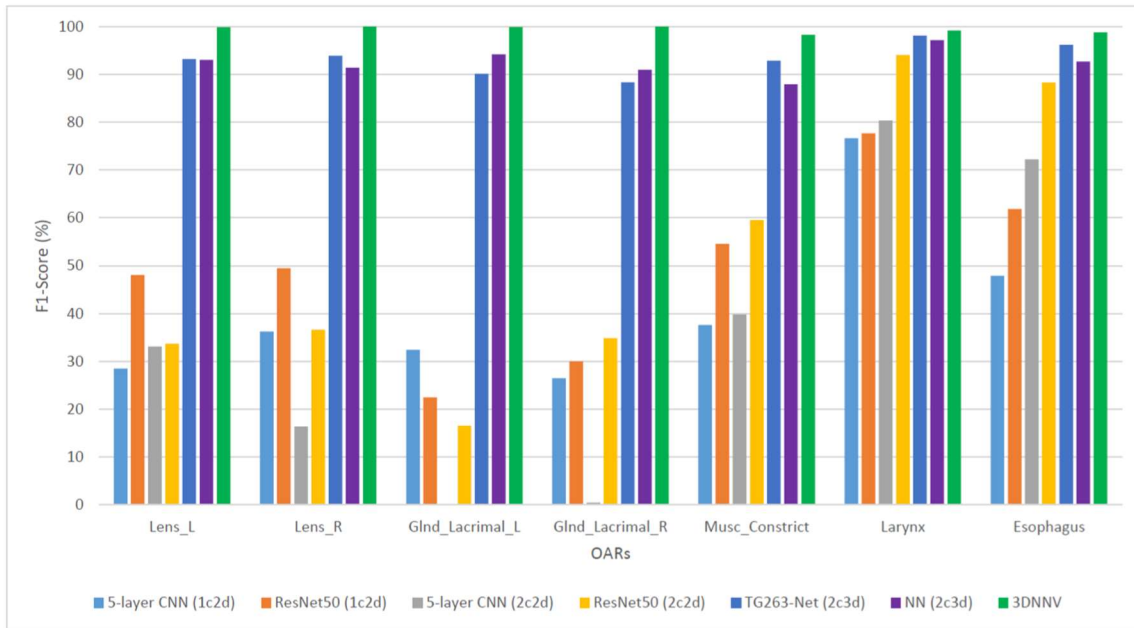


FIGURE 7. Average F1 Score (%) for small-volume OARs in HN_UTSW

not be applied to identifying the small-volume OARs, especially for Pituitary and OpticChiasm. The average TPR/F1 Score/AUC over all categories on all test datasets are shown in Table VI. Although TG263-Net

performed slightly better than Non-local Network on HN_UTSW, it took longer to run. Most importantly, 3DNNV outperformed the other DL-based methods with better generalizability on cross-institutional datasets.

TABLE VI
RESULTS COMPARING THE PERFORMANCE OF 3DNNV AND OTHER DL-BASED METHODS.

Architecture	HN PETCT			PDDCA			HN UTSW		
	TPR	F1	AUC	TPR	F1	AUC	TPR	F1	AUC
5-layer CNN [9] (1c2d)	74.28±22.88	73.57±23.20	86.82±11.46	58.61±36.58	62.65±33.63	78.78±18.27	57.10±25.63	55.62±22.34	77.87±12.61
ResNet50 [5] (1c2d)	74.86±25.18	75.08±25.21	87.13±12.61	60.37±36.55	62.92±32.06	79.45±18.02	60.41±28.54	56.42±21.88	79.55±13.98
5-layer CNN [9] (2c2d)	79.76±28.13	79.48±27.87	89.68±14.16	93.04±9.65	95.60±5.46	96.45±4.81	44.89±37.10	39.26±31.45	71.53±17.56
ResNet50 [5] (2c2d)	86.97±22.04	86.48±21.62	93.37±11.01	94.32±9.91	96.09±6.53	97.10±4.93	74.98±26.07	73.33±26.48	87.19±12.93
TG263-Net [35] (2c3d)	97.84±5.34	97.08±6.96	98.90±2.69	95.76±11.49	97.15±7.91	97.85±5.82	95.99±6.52	94.46±9.01	97.95±3.26
NN (2c3d)	94.27±14.17	91.72±15.85	97.02±7.09	89.12±31.10	89.78±29.86	94.55±15.58	91.36±12.83	89.58±18.19	95.58±6.49
3DNNV	99.81±0.63	99.82±0.39	99.90±0.31	100±0	100±0	100±0	98.87±2.37	98.90±1.91	99.42±1.19

TABLE VII
TESTING THE FINE-TUNED MODEL ON OTHER ANATOMICAL SITES (LUNGS AND PROSTATE).

Region	OARs	Train (samples)	Test (samples)	TPR (epoch=5)	TPR (epoch=7)	TPR (epoch=10)	TPR (epoch=20)
Lungs	Heart	8	30	63.33%	100.00%	100.00%	100.00%
	Carina	6	31	100.00%	100.00%	100.00%	100.00%
	Lungs	6	23	86.96%	100.00%	100.00%	100.00%
	Lung_L	6	26	3.85%	84.62%	96.15%	96.15%
	Lung_R	6	27	11.11%	96.30%	96.30%	96.30%
	Skin	2	3	100.00%	100.00%	100.00%	100.00%
Prostate	Rectum	5	30	100.00%	100.00%	100.00%	100.00%
	Bladder	5	29	89.66%	96.55%	96.55%	96.55%
	Sigmoid	4	21	19.05%	57.14%	71.43%	80.95%
	PenileBulb	4	25	52.00%	100.00%	100.00%	100.00%
	Femurs	3	12	100.00%	100.00%	100.00%	100.00%
	Femur_Head_L	2	20	100.00%	100.00%	100.00%	100.00%
	Femur_Head_R	2	20	100.00%	100.00%	100.00%	100.00%

D. 3DNNV's extensibility

To demonstrate the extensibility of the 3DNNV, we fine-tuned the model on other anatomical sites. Eight lung region

patients' data and 5 prostate region patients' data were selected for fine-tuning the model: we used the parameters of 3DNNV pre-trained on the 28 head-and-neck OAR data for initialization. We froze all parameters except those on the 4th residual block (Res4 shown in Fig. 4) and the fully-connected layer, and we set the learning rate as 1e-5 for the trainable layers. Then, we tested the fine-tuned model on 29 lung-region patients and 28 prostate-region patients. Other training settings were the same as those for 3DNNV.

The experimental results are shown in Table VII. Only 20 epochs were needed to transfer the model to recognizing OARs in other anatomical regions with a small amount of data, and a good recognition accuracy was obtained. This means that, with very little data and a short amount of time, we can easily transfer the pre-trained model to the target anatomical sites to meet the needs of the application.

V. DISCUSSION

A. Effectiveness of ASAC/voting strategy

Table II indicates that training the model on inputs generated by ASAC improves its performance at identifying OARs. So does the voting strategy. However, we still need to figure out why the ASAC/Voting strategy works for small-volume OARs. To this end, we visualized the predictive results of small-volume OARs in 3DNNV. As shown in Fig. 2, there are partial small-volume OARs in the head-and-neck region, the data of which are often poorly delineated and imbalanced. Furthermore, some of the small-volume OARs are similar in location and shape, such as Pituitary and OpticChiasm, Fig. 2 (c) shows that Pituitary and OpticChiasm are often confused with each other. With the voting strategy, we gained more reliable and credible results, as shown in Fig. 2 (d): clear boundaries between different categories that make it easier to classify.

B. Limitation

1) RUNNING TIME

To reduce the running time and improve the performance of 3DNNV, we added an early-match module (Fig. 8) to the framework and maintained a locally standardized label dictionary. The early-match module performs string matching [49] between the original label and the standardized label: if and only if the original label fully matches one of the standardized labels in the dictionary, then the standardized label is used to rename the given structure. As a result, the number of structures to be processed by 3DNNV is reduced, and the framework can process some unknown structures not included in the training dataset.

Originally, 3DNNV was used to process patient data containing 38 structures. A total of 7 m 41.83 s running time was required to obtain all the recognition results. For further applications, such a long running time is unacceptable. To solve this problem, we added the early-match module before feeding the input into the 3DNNV model. This module relies on a pre-stored dictionary as the basis for string matching. After adding the early-match module to the framework, only 17 OARs in this patient needed to be processed by 3DNNV,

and the total running time was 3 m 36.05s. Timely updates and maintenance for the dictionary will help to optimize the process of automatic identification and avoid reprocessing labels that have already been standardized. However, the limitation is that the dictionary can only handle one-to-one mapping. When given RT data collected from a multi-language environment, the dictionary mapping method will not significantly reduce the running time of standardization. This is why a single dictionary mapping method cannot handle cross-institutional data.

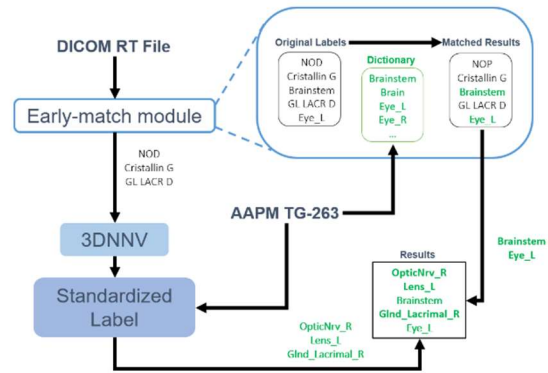


FIGURE 8. Early-match module.

2) MULTIPLE LABELS FOR THE SAME STRUCTURE

The original 3DNNV model was only trained and tested on 28 OARs in head-and-neck datasets, which limits the model's recognition range to these 28 categories. In order to make the model generalizable to more structures, we tried to extend the model to other anatomical sites, and it worked well. However, as mentioned in Schuler et al. [10], the model cannot distinguish typographic name variations from fundamental semantic differences in the same structure. In this work, we mainly discuss standardizing OAR labels, but in practice, the structures in individual RT data will be labeled differently for different treatment purposes; for example, the same structures might be labeled CavityOral_avoid or CavityOral, SpinalCord or SpinalCord_5mm, IL_Parotid, CL_Parotid, Parotid_L, or Parotid_R, etc., depending on the specific application for which the labels are being used. These inputs have similar semantic features in images, therefore it is very difficult to identify these structures based on image information. At the same time, some non-target structures will have multi-level labels for a single OAR—such as Musc_Constrict_M, Musc_Constrict_S, Musc_Constrict_I, and Musc_Constrict—depending on different RT plans and clinicians' preferences. These standardization conventions may vary across different medical institutions and different treatment plans. At the same time, the standardization of target volumes is also worthy of attention. The target volume often overlaps with OARs and is misidentified as an OAR. In different RT plans, the delineation for PTV/CTV/GTV varies, and standardizing labels for the target volume will be a challenging task. Combining text information on labels, dose distribution, and image

information may help us to improve the performance of 3DNNV and meet the requirements of clinical applications.

3) OUTLIER

In previous experiments, we found that the masks collected from different clinical centers may have inconsistent contours, which actually depends on the definition of delineation for OARs and the experience of physicians in the local institution. Moreover, there are outliers in many datasets, such as lack of masks in some slices, or the label does not always match with the contour in the mask (such as inaccurate delineation and partial depictions). We believe that detecting delineation outliers also presents a challenge to standardizing nomenclature for RT data.

VI. CONCLUSIONS

In this paper, we propose a novel framework, 3DNNV, that combines an ASAC/Voting strategy and a non-local network to integrate clinicians' domain knowledge and recognition mechanisms into our deep learning architecture. To the best of our knowledge, our work is the first to propose an architecture with domain knowledge to solve the recognition problems caused by imbalance and poor delineation. Our model had a significantly higher average TPR than the baseline model across the three test datasets (+ 8.27%, + 2.39%, + 5.53%). More importantly, our model outperformed the baseline, 28.63% to 91.17%, in terms of the F1 Score of the Pituitary with only 9 training samples, when tested on the HN_UTSW dataset. This work will lead to the automated standardization of organ labels in DICOM RT data which is important for data driven research.

REFERENCES

- [1] Y. LeCun, et al., "Gradient-based learning applied to document recognition," in *Proceedings of the IEEE*, vol. 86, no. 11, pp. 2278-2324, Nov. 1998. DOI: 10.1109/5.726791, [Online].
- [2] R. Battiti, A. M. Colla, "Democracy in neural nets: Voting schemes for classification," *Neural Networks*, vol. 7, no. 4, pp. 691-707, 1994, DOI: 10.1016/0893-6080(94)90046-9, [Online].
- [3] C. L. Brouwer, et al., "CT-based delineation of organs at risk in the head and neck region: DAHANCA, EORTC, GORTEC, HKNPCSG, NCIC CTG, NCR1, NRG Oncology and TROG consensus guidelines," *Radiotherapy and Oncology*, vol. 117, no. 1, pp. 83-90, 2015, DOI: 10.1016/J.RADONC.2015.07.041, [Online].
- [4] K. Clark, B. Vendt, K. Smith, et al., "The cancer imaging archive (tcia): Maintaining and operating a public information repository" *Digit Imaging*, vol. 26, no. 6, pp. 1045-1057, 2013, DOI:10.1007/S10278-013-9622-7, [Online].
- [5] K. He, et al. "Deep residual learning for image recognition," in *CVPR*, Las Vegas, Nevada, USA, 2016, pp. 770-778.
- [6] C. S. Mayo, T. M. Pisansky, I. A. Petersen, et al. "Establishment of practice standards in nomenclature and prescription to enable construction of software and databases for knowledge-based practice review," *Practical Radiation Oncology*, vol. 6, no. 4, pp. e117-e126, 2016. DOI: 10.1016/J.PRRO.2015.11.001, [Online].
- [7] C. S. Mayo, et al. "American association of physicists in medicine task group 263: Standardizing nomenclatures in radiation oncology," *International Journal of Radiation Oncology*Biophysics*Physics*, vol. 100, no. 4, pp. 1057-1066, Mar. 2018, DOI: 10.1016/J.IJROBP.2017.12.013, [Online].
- [8] P. F. Raudaschl, et al., "Evaluation of segmentation methods on head and neck CT: Auto-segmentation challenge 2015," *Medical physics*, vol. 44 no. 5, pp. 2020-2036, Jun. 2017, DOI: 10.1002/MP.12197, [Online].

- [9] T. Rozario, T. Long, M. Chen, W. Lu, S. Jiang, "Towards automated patient data cleaning using deep learning: A feasibility study on the standardization of organ labeling," *arXiv.org*, Dec. 2017, [Online], Available: <https://arxiv.org/abs/1801.00096>
- [10] T. Schuler, J. Kipritidis, T. Eade, et al. "Big data readiness in radiation oncology: An efficient approach for relabeling radiation therapy structures with their tg-263 standard name in realworld data sets," *Advances in Radiation Oncology*, vol. 4, no. 1, pp. 191-200, 2019, DOI: 10.1016/J.ADRO.2018.09.013, [Online].
- [11] K. Simonyan and A. Zisserman, "Very deep convolutional networks for large-scale image recognition," In *ICLR*, San Diego, CA, USA, 2015.
- [12] M. Vallières, E. Kay-Rivest, et al. "Radiomics strategies for risk assessment of tumour failure in head-and-neck cancer," *Scientific Reports*, no. 7:10117, 2017, DOI: 10.1038/S41598-017-10371-5, [Online].
- [13] M. Vallières, et al. "Data from Head-Neck-PET-CT," the *Cancer Imaging Archive*, 2017, DOI: 10.7937/K9/TCIA.2017.8OJE5Q00, [Online], Available: <https://wiki.cancerimagingarchive.net/display/Public/Head-Neck-PET-CT>
- [14] A. Vaswani, N. Shazeer, et al., "Attention is all you need," in *NeurIPS*, Long Beach, CA, USA, 2017, pp. 5998-6008.
- [15] X. Wang, et al., "Non-local neural networks," in *CVPR*, Salt Lake City, Utah, USA, 2018, pp. 7794-7803.
- [16] W. Zhu, Y. Huang, et al. "AnatomyNet: Deep learning for fast and fully automated whole-volume segmentation of head and neck anatomy," *Medical physics*, vol. 46, no. 2, pp. 576-589, Nov. 2018, DOI: 10.1002/MP.13300, [Online].
- [17] A. Krizhevsky, et al., "ImageNet Classification with Deep Convolutional Neural Networks" in *NIPS*, Lake Tahoe, Nevada, USA, 2012, pp. 1097-1105.
- [18] S. Xie, et al., "Aggregated Residual Transformations for Deep Neural Networks" in *CVPR*, Honolulu, Hawaii, USA, 2017, pp. 1492-1500.
- [19] S. Gao, M. Cheng, K. Zhao, et al., "Res2Net: A New Multi-Scale Backbone Architecture" in *IEEE TPAMI*, 2020, DOI: 10.1109/TPAMI.2019.2938758, [Online].
- [20] G. Huang, Z. Liu, et al., "Densely Connected Convolutional Networks" in *CVPR*, Honolulu, Hawaii, USA, 2017, pp. 4700-4708.
- [21] Q. Dou, H. Chen, L. Yu, et al., "Multilevel Contextual 3-D CNNs for False Positive Reduction in Pulmonary Nodule Detection" *IEEE Transactions on Biomedical Engineering*, vol. 64, no. 7, pp. 1558-1567, Jul. 2017, DOI: 10.1109/TBME.2016.2613502, [Online].
- [22] S. Bianco, et al., "Benchmark Analysis of Representative Deep Neural Network Architectures" *IEEE Access*, vol. 6, pp. 64270-64277, Oct. 2018, DOI: 10.1109/ACCESS.2018.2877890, [Online].
- [23] L. Potters, E. Ford, S. Evans, T. Pawlicki, S. Mutic "A systems approach using big data to improve safety and quality," *International Journal of Radiation Oncology • Biology • Physics*, vol. 95, no. 3, pp. 885-889, Jul. 2016, DOI: 10.1016/J.IJROBP.2015.10.024, [Online].
- [24] D. Hultstrom, "Standards for cancer registries volume II: Data standards and data dictionary" *North American of Central Cancer Registries*, edition 7th, version 10, Mar. 2002, [Online] Available: <https://www.naacr.org/wp-content/uploads/2016/12/NAACCR-Volume-II-REVISED-5-14-02.pdf>
- [25] L. Santanam, C. Hurkmans, et al. "Standardizing naming conventions in radiation oncology," *International Journal of Radiation Oncology*Biophysics*Physics*, vol. 83, no. 4, pp. 1344-1349, Jul. 2012, DOI: 10.1016/J.IJROBP.2011.09.054, [Online].
- [26] S. P. Robertson, H. Quon et al. "A data-mining framework for large scale analysis of dose-outcome relationships in a database of irradiated head and neck cancer patients," *Medical Physics*, vol. 42, no. 7, pp. 4329-4337, Jun. 2015, DOI: 10.1118/1.4922686, [Online].
- [27] J. O. Deasy, S. M. Bentzen, et al. "Improving normal tissue complication probability models: The need to adopt a 'data-pooling' culture," *International Journal of Radiation Oncology*Biophysics*Physics*, vol. 76, no. 3, pp. S151-S154, Mar. 2010, DOI: 10.1016/J.IJROBP.2009.06.094, [Online].
- [28] E. Roelofs, A. Dekker, E. Meldolesi, et al. "International data-sharing for radiotherapy research: An open-source based infrastructure for multicentric clinical data mining," *Radiotherapy and Oncology*, vol.

- 110, no. 2, pp. 370-374, Feb. 2014, DOI: 10.1016/J.RADONC.2013.11.001, [Online].
- [29] R. C. Chen, et al. "How will big data impact clinical decision making and precision medicine in radiation therapy?" *International Journal of Radiation Oncology • Biology • Physics*, vol. 95, no. 3, pp. 880 – 884, Jul. 2016, DOI: 10.1016/J.IJROBP.2015.10.052, [Online].
- [30] T. Skripcak, C. Belka, W. Bosch, et al. "Creating a data exchange strategy for radiotherapy research: Towards federated databases and anonymised public datasets," *Radiotherapy and Oncology*, vol. 113, no. 3, pp. 303-309, Dec. 2014, DOI: 10.1016/J.RADONC.2014.10.001, [Online].
- [31] T. Nyholm, C. Olsson, M. Agrup, et al. "A national approach for automated collection of standardized and population-based radiation therapy data in Sweden" *Radiotherapy and Oncology*, vol. 119, no. 2, pp. 344-350, 2016, DOI: 10.1016/J.RADONC.2016.04.007, [Online].
- [32] C. S. Mayo, M. L. Kessler, et al. "The big data effort in radiation oncology: Data mining or data farming?" *Advances in Radiation Oncology*, vol. 1, no. 4, pp. 260-271, 2016, DOI: 10.1016/J.ADRO.2016.10.001, [Online].
- [33] A. Sotiras, et al., "Deformable medical image registration: A survey," *IEEE Transactions on Medical Imaging*, vol. 32, no. 7, pp. 1153-1190, 2013, DOI:10.1109/TMI.2013.2265603, [Online].
- [34] H. Duc, "Atlas-Based Methods in Radiotherapy Treatment of Head and Neck Cancer" Doctoral thesis, University College London, London, UK, 2013.
- [35] D. Rhee, C. Nguyen, T. Netherton, et al., "TG263-Net: A Deep Learning Model for Organs-At-Risk Nomenclature Standardization" Presented as e-poster at the AAPM 61st Annual Meeting, San Antonio, TX, USA, Jul. 14-18, 2019
- [36] F. Milletari, N. Navab and S. Ahmadi, "V-Net: Fully Convolutional Neural Networks for Volumetric Medical Image Segmentation," in 2016 Fourth International Conference on 3D Vision (3DV), Stanford, CA, USA, 2016, pp. 565-571, DOI: 10.1109/3DV.2016.79.
- [37] K. He, et al., "Delving Deep into Rectifiers: Surpassing Human-Level Performance on ImageNet Classification" in ICCV, Santiago, Chile, 2015, pp. 1026-1034.
- [38] H. Wickham, "Tidy data," *Journal of Statistical Software*, vol. 59, no. 10, pp. 1-23, Aug. 2014. [Online], Available: <https://www.jstatsoft.org/article/view/v059i10/v59i10.pdf>
- [39] T. Dasu, T. Johnson, "Data Quality," in *Exploratory Data Mining and Data Cleaning*, New York, NY, USA: John Wiley & Sons, Inc., 2003
- [40] R. Novak, Y. Bahri, et al., "Sensitivity and generalization in neural networks: an empirical study," in ICLR, Vancouver, BC, Canada, 2018.
- [41] R. Geirhos, P. Rubisch, et al., "ImageNet-trained CNNs are biased towards texture; increasing shape bias improves accuracy and robustness," in ICLR, New Orleans, Louisiana, USA, 2019.
- [42] Tiange Luo, et al., "Few-Shot Learning with Global Class Representations" in ICCV, Seoul, Korea, 2019.
- [43] J. Sivic, B. C. Russell, et al., "Discovering object categories in image collections," in ICCV, Beijing, China, 2005, pp. 2254-2261.
- [44] B. E. Boser, et al., "A training algorithm for optimal margin classifiers," in Fifth Annual Workshop on COLT, Pittsburgh, Pennsylvania, USA, 1992, pp. 144-152.
- [45] T. Lin, P. Goyal, R. Girshick, K. He and P. Dollár, "Focal Loss for Dense Object Detection," in ICCV, Venice, Italy, 2017, pp. 2980-2988
- [46] D. P. Kingma and J. Ba, "Adam: A Method for Stochastic Optimization," in ICLR, San Diego, CA, USA, 2015.
- [47] G. Mariani, F. Scheidegger, R. Istrate, C. Bekas, and C. Malossi. "BAGAN: Data augmentation with balancing GAN," arXiv preprint arXiv:1803.09655, 2018.
- [48] Ekin D. Cubuk, et al., "AutoAugment: Learning Augmentation Policies from Data" in CVPR, Long Beach, CA, USA, 2019, pp. 113-123.
- [49] Fuzzywuzzy [Online]. Available: <https://github.com/seatgeek/fuzzywuzzy>



Qiming Yang received the B.S. degree in software engineering from the Sun Yat-sen University, Guangzhou, China, in 2017. Her previous works focused on biomedical image processing. She is currently pursuing the M.S. degree in Sun Yat-sen University and was visiting the University of Texas Southwestern Medical Center in Dallas, Texas, from September 2018 to August 2019. Her research interests include image processing, deep learning, and computer vision.



Hongyang Chao received the B.S. and Ph.D. degrees in computational mathematics from Sun Yat-sen University, Guangzhou, China. In 1988, she joined the Department of Computer Science, Sun Yat-sen University, where she was initially an Assistant Professor and later became an Associate Professor. She is currently a Full Professor in the School of Data and Computer Science. She has published extensively in the area of image/video processing and holds 3 U.S. patents and 4 Chinese patents in the related area. Her current research interests include image and video processing, image and video compression, massive multimedia data analysis, and content-based image (video) retrieval. She was visiting the University of Texas Southwestern Medical Center in Dallas, Texas, from September 2018 to August 2019.



Dan Nguyen is currently an Assistant Professor in the Medical Artificial Intelligence and Automation (MAIA) Laboratory at the University of Texas Southwestern Medical Center in Dallas, Texas. He received a B.S. in Physics at the University of Texas at Austin in 2012 and Ph.D. in Biomedical Physics at the University of California, Los Angeles in 2017. His current research in MAIA Lab includes using artificial intelligence technologies and advanced optimization algorithms for radiation therapy treatment planning. In particular he is tackling problems involving clinical volumetric dose prediction, Pareto surface navigation, incorporating human and learned domain knowledge, dose calculation, beam orientation optimization, and uncertainty estimation.



Steve Jiang received his Ph.D. in Medical Physics from Medical College of Ohio in 1998. After completing his postdoctoral training at Stanford University, he joined Massachusetts General Hospital and Harvard Medical School in 2000 as an Assistant Professor of Radiation Oncology. In 2007, Dr. Jiang was recruited to University of California San Diego as a tenured Associate Professor to build Center for Advanced Radiotherapy Technologies, for which he was the founding and executive director. He was then promoted to Full Professor with tenure in 2011. In October 2013, Dr. Jiang joined University of

Texas Southwestern Medical Center as a tenured Full Professor, Barbara Crittenden Professor in Cancer Research, Vice Chair of Radiation Oncology Department, and Director of Medical Physics and Engineering Division. He is the founding director for Medical Artificial Intelligence and Automation Laboratory. Dr. Jiang is a Fellow of Institute of Physics and American Association of Physicists in Medicine. His current research interest is to develop and deploy artificial intelligence technologies to solve medical problems.